International Journal of GEOMATE, July, 2024 Vol.27, Issue 119, pp.34-41
ISSN: 2186-2982 (P), 2186-2990 (O), Japan, DOI: https://doi.org/10.21660/2024.119.4361
Geotechnique, Construction Materials and Environment

SHEAR-TENSION BEHAVIOR OF FIBER-REINFORCED CONCRETE: A FINITE ELEMENT STUDY USING THE INCLINED PUSH-OFF TEST MODEL

Mudji Irmawan[1], *Bambang Piscesa[1], Indra Komara[2], Danny Triputra Setiamanah[1], Witantyo Witantyo[3], Dwi Agus Purnomo[4], Djoko Prijo Utomo[4], and Wimpie Agoeng Noegroho Aspar[4]

[1]Department of Civil Engineering, Institut Teknologi Sepuluh Nopember, Indonesia;
[2]Department of Civil Engineering, Institut Teknologi Adhi Tama Surabaya, Indonesia;
[3]Department of Mechanical Engineering, Institut Teknologi Sepuluh Nopember, Indonesia;
[4]Research Center for Transportation Technology, BRIN, Jakarta, Indonesia

*Corresponding Author, Received: 05 Jan. 2024, Revised: 6 Feb. 2024, Accepted: 20 May 2024

ABSTRACT: This paper uses numerical simulation to investigate the behavior of fiber-reinforced concrete tested under combined shear and tension. The test setup was based on an inclined push-off test. The numerical simulation was carried out using an in-house finite element package that employs the multi-surface plasticity model for concrete material. Three fiber materials are being investigated: steel fiber, polypropylene fiber (PP), and polyvinyl alcohol fiber (PVA). The stress-strain model for each fiber material was obtained from the laboratory test. The accuracy of the finite element (FE) model was first validated with the available reinforced concrete specimen that was being tested under a push-off test. The numerical simulation found that the push-off model made with steel-fiber reinforced concrete (SFRC) responds similarly to plain reinforced concrete (RC) but with a 72.48 % increase in load-carrying capacity. For the PVA-ECC FRC, the load-carrying capacity at the peak displacement of 5.20 mm increased to more than 113.78 %. On the other hand, using PP-FRC can only slightly increase the load-carrying capacity by 8.28 %. In addition, the PP-FRC has a much softer response during hardening due to lower elastic modulus than plain concrete.

Keywords: Push-off test, Shear-tension failure, Nonlinear finite element, Fiber-reinforced concrete, Plasticity-Fracture model

1. INTRODUCTION

The enhancement of concrete's fundamental material properties has been the subject of extensive research, with a notable approach involving incorporating embedded fibers into the concrete matrix. Whether synthetic or steel-based, these fibers improve tensile strength, compressive strength, and ductility [1–5]. Beyond these fundamental enhancements, fiber-reinforced concrete (FRC) has demonstrated its efficacy in enhancing crack resistance [6], toughness and durability [7], the bond strength between steel bars and concrete [8], and overall energy dissipation, leading to potential cost-effectiveness in construction.

While the benefits of FRC have been acknowledged, a significant challenge in its application, particularly in construction, has been the quality control of the mixing process in the field [9]. Despite this challenge, research on using fibers in concrete has been ongoing for decades, primarily focusing on structures vulnerable to shear failures, such as concrete bridge deck collapses [10,11], shear in reinforced concrete beams [12], torsion in reinforced concrete beams [13], and corbel failures [14]. However, limited attention has been given to structural elements experiencing combined shear and tension loads.

In plain concrete structural elements subjected to combined shear and tension, tension within the shear plane significantly reduces the shear strength capacity of the element. To address this issue, some studies, such as Foster et al.'s [15], have explored experimental tests to enhance shear strength capacity by introducing CFRP fabric to restrain crack growth. However, the focus has primarily been on increasing tensile strength externally using CFRP and using embedded fiber in concrete to enhance both tensile and shear strength has been explored less.

This paper aims to fill this research gap by investigating fiber-reinforced concrete's shear strength enhancement potential in elements subjected to combined shear and tension loads. Unlike the traditional approach of externally strengthening with CFRP, the focus here is on increasing the tensile strength of concrete through embedded fibers. This method is expected to provide a more uniform strength distribution in the shear-critical area, potentially overcoming issues associated with debonding failure between CFRP and the concrete surface.

Fiber-reinforced concrete exhibits both softening and hardening responses, and variations in macroscopic characteristics may influence its performance. Consequently, adjustments in existing concrete constitutive models may be necessary. The

paper employs a validated stress-strain model to predict the response of a push-off test, assessing the shear strength enhancement achievable by using FRC to improve the tensile strength properties of concrete.

The investigation involves three different FRCs and stress-strain data obtained from experimental tests are utilized to characterize their basic tensile properties. The performance of each FRC is then scrutinized using a push-off test framework modeled through nonlinear finite element analysis.

The paper is structured into seven sections, covering introduction, research significance, an overview of the in-house finite element package, detailed test setup and material properties, discussion on behavior and input materials for plain and fiber-reinforced concrete, analysis of the numerical model and results, and a conclusive summary of findings obtained from the analysis.

2. RESEARCH SIGNIFICANCE

This research investigates the performance of different fiber-reinforced concrete under combined shear and tension. The push-off test configuration was used, and the plain reinforced concrete specimen was verified with the available test result in the literature. A detailed comparison and explanation of the stress-strain model was made between the FRC and plain concrete. An inverse analysis was carried out for each of the stress-strain models from the experimental test of three-point bending notched beam for steel fiber reinforced concrete (SFRC) and four-point bending for polypropylene fiber reinforced concrete (PP-FRC) and polyvinyl alcohol engineered cementitious composite fiber reinforced concrete (PVA-ECC). The fracture parameters that represent the anticipated cracking pattern in the model, as well as comparisons and in-depth explanations of the load-deflection curves for each model, are also included in the papers.

3. FINITE ELEMENT PACKAGE

An in-house finite element package called 3D-NLFEA software is used for the finite element analysis [17–19]. A few critical steps must be taken to begin gathering data: the geometry must be defined, boundary constraints must be assigned, and the meshing must be established. SALOME 9.11 was used in the pre-processor phase. The steel plate support was assigned as hinges such that rotation was allowed.

The 3D-NLFEA package uses the multi-surface plasticity model that combines the Menetrey and Willam failure surfaces [20] for concrete under compression and tension cut-off failure surface for concrete under tension [21]. The flow rule for concrete under compression is non-associative [22–27], and for tension, it is associative. The stress-crack opening model for concrete under tension was converted into strain using the internal length scale [28,29].

4. PUSH-OFF SPECIMEN TEST SETUP AND MATERIAL PROPERTIES

Fig. 1a shows the typical push-off specimen geometry from Foster et al. [15], where the specimen ID is C/S2/F0. The critical shear region was added with two close loop stirrups bars with a diameter equal to 6 mm. The pitch spacing of the bars is 75 mm. The thickness of the push-off specimen in the out-of-plane direction is 250 mm.

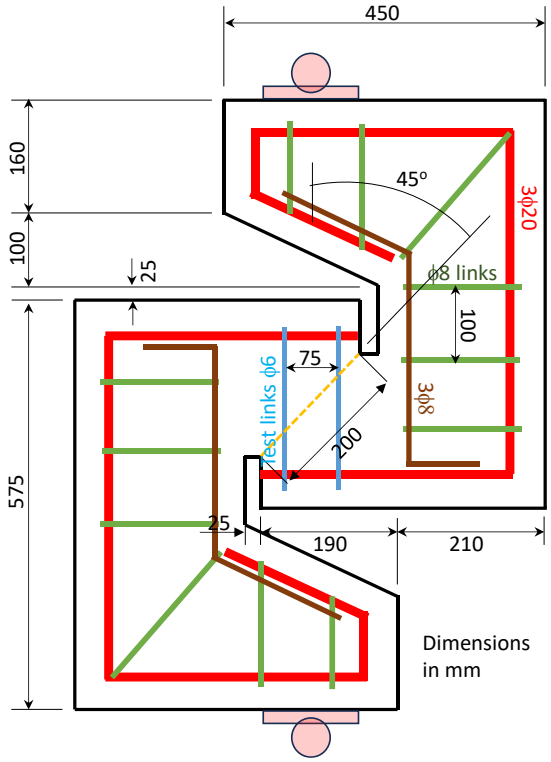

(a)

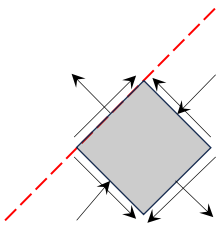

(b)

Fig.1 Push-off geometry details and boundary conditions [all dimensions are in millimeters]: (a) Geometry details [15]; (b) forces that act on the diagonal crack surface

With the current configuration, the shear critical region is inclined about 45 degrees with the horizontal axis. It is expected that the forces that act on the critical section are a combination of tensile and sliding shear forces, as shown in Fig. 1b. The steel

plate was placed at both ends and is a hinged type of support where rotation is permitted. The load is given using displacement control. It is expected that no snap-back behavior was observed from the test, such that using the arc-length method [30] in the finite element analysis was unnecessary, and complete conjugate displacement control was used in the numerical simulation.

The concrete compressive strength is 50 MPa, and the tensile strength is 3.2 MPa. The 6 mm diameter stirrups that cross the shear plane have a yield strength minimum of 275 MPa or equivalent to S275. The behavior of the rebar is assumed to behave as an elastic-perfect plastic material without rupture. The meshed geometry of the push-off test was prepared using SALOME 9.11 [31].

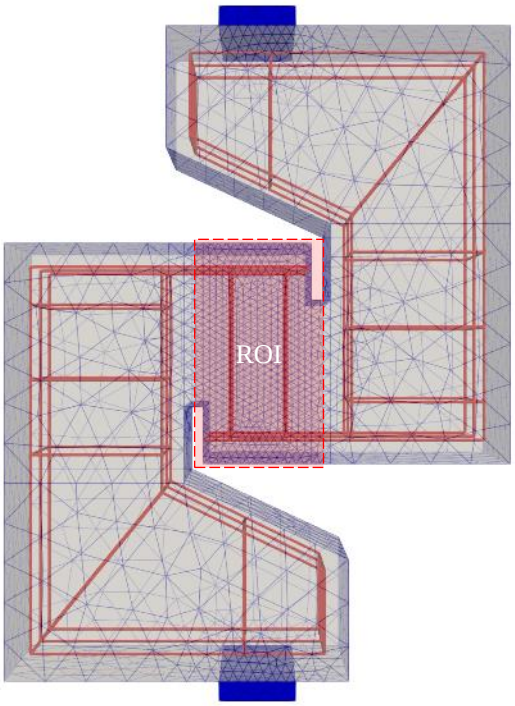

Fig.2 Meshed model of the push-off specimen

Fig. 2 shows the meshed 3D model of the push-off specimen. The geometry was meshed using a four-node tetrahedral element. BBar element technology that differentiated the hydrostatic and deviatoric part of the B-Matrix during integration [32] was used to prevent volumetric locking. From the pre-processor phase, the total number of nodes is 15,480, and the total number of tetrahedral elements is 80,305. The area around the shear plane was meshed with a much smaller mesh than the rest of the area, which is expected to have crack localization. The area is noted as the region of interest (ROI, [33]).

The steel reinforcing bar was modeled using embedded elements [34,35] such that the deformation will follow the parent element deformation. The total nodes and elements for the rebar are 2,154 and 2,276, respectively. It should be noted that in 3D-NLFEA, the rebar is then meshed according to the mesh of the parent elements such that the total number of nodes and elements will be greater than the meshed number from the pre-processor phase.

5. BEHAVIOR OF PLAIN, STEEL-FIBER, PP-FIBER, AND PVA-FIBER CONCRETE

The tensile splitting test was used to determine the tensile strength of plain concrete, and the CEB-FIP Model Code 1990 was used to determine the fracture energy [36]. A bilinear softening function was utilized in the stress-strain model for plain concrete, as suggested by Hoover and Bažant [28]. (see Fig. 3a). The tensile fracture energy of the plain concrete is the area beneath the stress-crack opening displacement curve. The stress-strain model for steel fiber-reinforced concrete (SFRC), taken from [37], is depicted in Fig. 3b.

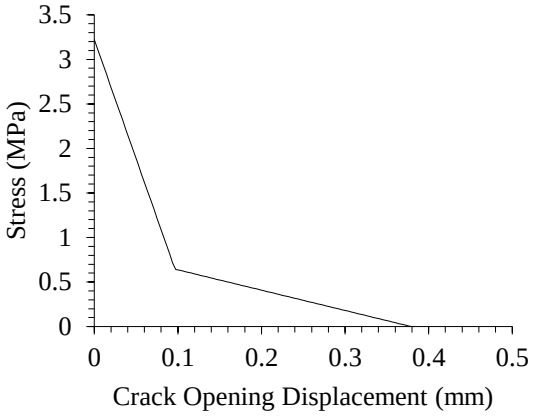

(a)

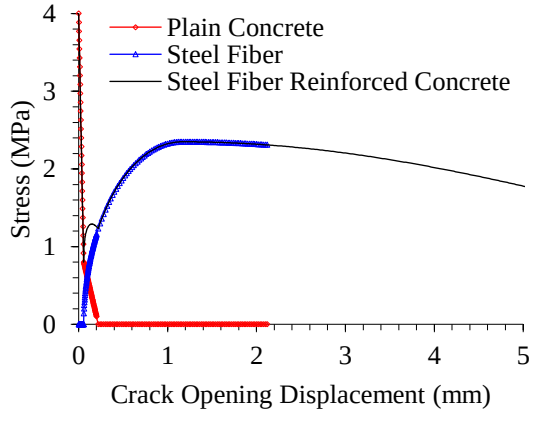

(b)

Fig. 3. Input for the stress-strain model in the 3D-NLFEA package: (a) Plain Concrete; (b) Steel Fiber Reinforced Concrete

Using the inverse analysis of the test result of the three-point bending of the SFRC notched beam with volumetric fiber content (V_f) equal to two percent, the model parameters in [37] are customized. The steel fiber is a Dramix 4D 65/60 BG produced by

BEKAERT. Steel fiber's nominal tensile strength, elastic modulus, and ultimate strain are 1600 MPa, 200 GPa, and 0.8%, respectively. The fiber length is 60 mm, and the fiber diameter is 0.9 mm. The ratio of length over the diameter (l/d) is 65.

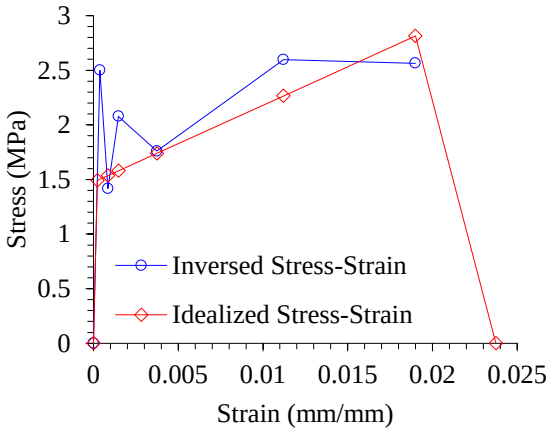

(a)

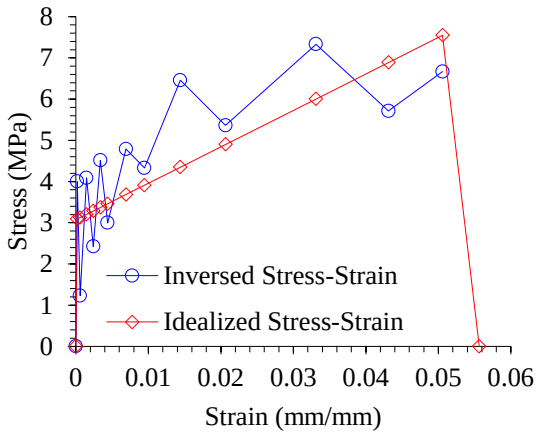

(b)

Fig. 4. Input for the stress-strain model in the 3D-NLFEA package: (a) Polypropylene Fiber Reinforced Concrete (1.25%) Elongated up to 49.14 ε_t; (b) Polyvinyl Alcohol Fiber Reinforced Concrete (1.25%) Elongated up to 275.1 ε_t

The Type of PP fiber is Mapefibre NS12 with a diameter of 32 μm, length of 12 mm, density of 0.91 g/cm^3, tensile strength of 400~500 MPa, and elastic modulus of 3.5 GPa. On the other hand, the type of PVA fiber is REC15, which has a diameter of 40 mm, a length of 12 m, a density of 1.3 g/cm^3, a tensile strength of 1,600 MPa, and an elastic modulus of 41 GPa. From the mechanical properties of PP and PVA fibers, it was clear that the elastic modulus for PP fibers is far less than the PVA fibers, such that it is expected that the PP-FRC concrete would have a lower elastic modulus compared to PVA fibers.

The stress-crack opening displacement was obtained from inverse analysis of the four-point bending prism test [38] (see Figs. 4a and 4b) for PP and PVA fiber-reinforced concrete. The blue dotted line in Figs. 4a and 4b were the inverse analysis results for the stress-crack opening displacement. The obtained stress-crack opening displacement is then idealized as a trilinear stress-crack opening displacement shown as the red dotted line in Figs. 4a and 4b.

The input data for concrete under tension that employs crack opening displacement (plain concrete and steel fiber reinforced concrete) is converted into the fracturing strain by dividing the crack opening displacement by the internal length scale (L_T) as in the smeared crack model ($\Delta_{COD} = L_T \times \varepsilon_f$). In contrast, the input data that uses the total tensile strain must be converted to the fracturing strain and divided by the internal length scale from the test specimen to translate the fracturing strain into the crack-opening displacement. PP and PVA fibers share almost similar macroscopic appearances. However, both fibers behave differently. Besides the vast difference in elastic modulus between two fibers, the maximum elongation between fibers also differs significantly. The PP-FRC can only be elongated up to 49.14 times the peak strain, while the PVA-FRC can be elongated up to 275.1 times the peak strain. The volumetric fiber content for both PP-FRC and PVA-FRC is 1.25 %.

6. NUMERICAL MODEL RESULTS AND DISCUSSIONS

Table 1 summarizes the finite element simulation results for the push-off test with various FRC configurations and conventional RC ones. Fig. 5 shows the load-deformation curve of the modeled push-off specimen. The push-off test from the literature for plain reinforced concrete was also shown in Fig. 5. As shown in Fig. 5, the prediction for the peak, the sharp softening curve, and the residual load level of the plain RC using 3D-NLFEA were in good agreement with the test result. The peak load from the test result is 132.06 kN at the peak displacement of 1.52 mm. The predicted peak load for the plain RC push-off specimen was 123.31 kN at the peak displacement of 1.48 mm. The peak load prediction from the numerical model was 6.62 % lower than the test results, and the ascending of the load-deflection response was slightly stiffer than the test results. The shape of the load-deformation curve for plain RC and SFRC push-off models was somewhat similar. It does have one peak, sharp softening once the concrete cracks, and a residual load level that shows the pure contribution from the reinforcing bar at yield, and some portion of the fiber resisted the crack growth. The predicted residual load for the plain RC push-off specimen is 46.91 kN, measured when the displacement is 2.32 mm. The predicted residual load is lower than the test result,

which showed a residual load value equal to 52.493 kN at a displacement of 5.00 mm.

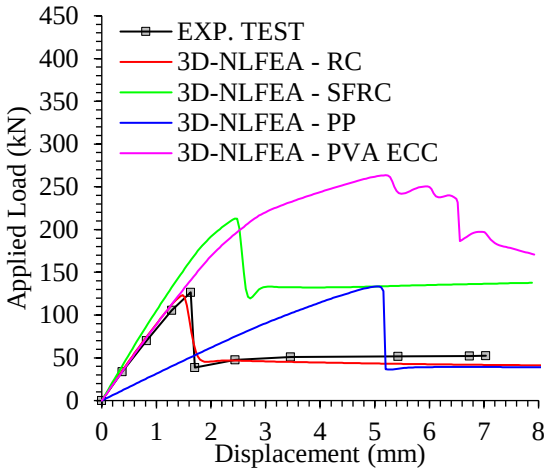

Fig. 5. Load-displacement response for the FRC push-off specimens

The behavior of the SFRC push-off specimen tends to have a stiffer response, and the peak load carrying capacity reached 212.68 %, about 72.48% higher than the plain conventional RC. The stiffer response is contributed by the high elastic modulus of the steel fiber compared to the concrete. Once the peak load was reached, the concrete cracks and the crack restraining mechanism took place such that it would lead to a higher residual load compared to the plain RC push-off specimen. The residual load of the SFRC push-off specimen is 135.19 kN, which is about 188.19% higher than that of the plain RC push-off specimen.

Table 1 Summary of the FE simulation for the push-off test

Material	Peak Load (kN)	Peak Deformation (mm)	Residual Load (kN)
Conventional RC	123.31 (+0.00% Ref.)	1.48 (+0.00% Ref.)	46.91 (+0.00% Ref.)
Steel FRC	212.68 (+72.48%)	2.48 (+67.57%)	135.19 (+188.19%)
Polypropylene FRC	133.51 (+8.28%)	5.04 (+240.54%)	-
Polyvinyl Alcohol FRC	263.61 (+113.78%)	5.20 (+251.35%)	-

The performance of the PP-FRC push-off specimen was somewhat unsatisfactory as it reduced the concrete modulus quite significantly and did not significantly increase the specimen's load-carrying capacity. The peak load-carrying capacity of the PP-FRC is 133.51 kN, which is about 8.28% higher than that of the plain RC push-off specimen. With the deformation at peak load reaching 5.04 mm, the elastic modulus of the PP-FRC was 3.51 times lower than the plain RC push-off specimen. After the fiber breaks, sudden drops in the load-carrying capacity were observed and reduced to almost the same residual level as the plain RC push-off specimen.

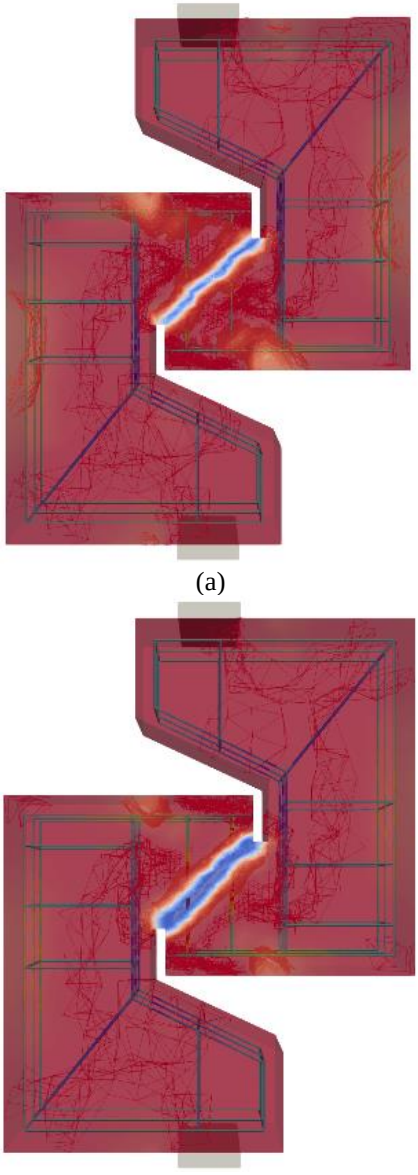

(a)

(b)

Fig. 6. Fracturing parameter contour of the 3D-NLFEA model: (a) Plain RC; (b) SFRC

The load-deformation curve for the PVA-ECC FRC push-off model showed an excellent response where a ductile behavior was formed. Once it reaches the peak load of 263.61 kN, which was 113.78% higher than the plain RC push-off specimen, at a displacement of 5.20 mm, the curve drops, indicating that the fiber breaks gradually as it was not observed such a sharp failure pattern as in any other push-off specimen.

Fig. 6a shows the detailed crack pattern for plain RC. As shown in Fig. 6a, the cracks were formed diagonally, and the crack bandwidth was localized. The crack pattern for SFRC was like the plain RC specimen. However, one can notice that the width of

the SFRC push-off specimen's crack band was more expansive than the plain RC ones, indicating that the steel fiber could resist the crack growth and resulted in a broader crack bandwidth.

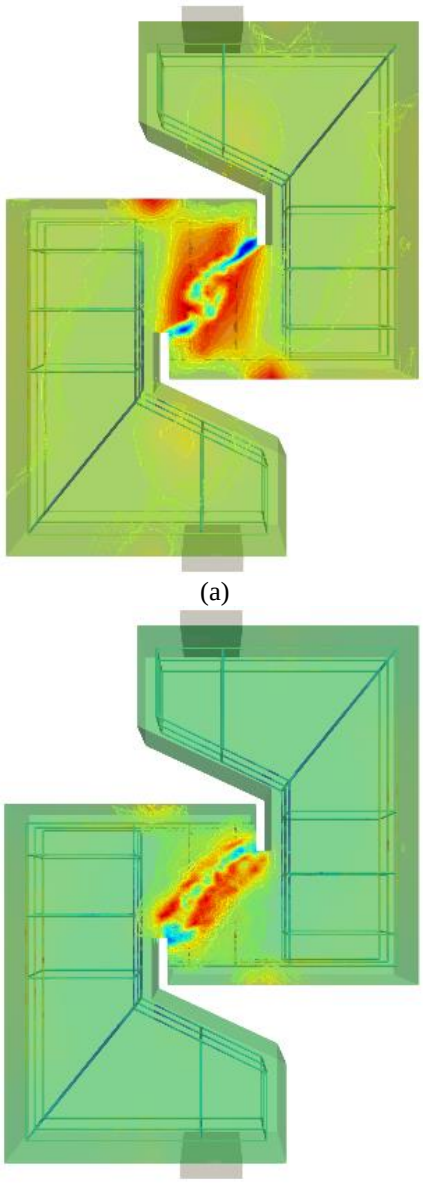

(a)

(b)

Fig. 7. Fracturing parameter contour of the 3D-NLFEA model: (a) PP-FRC; (b) PVA-ECC

For PP-FRC, as shown in Fig. 7a, the fracturing contour was localized near the edge but did some propagation away from the crack localized area. The significant crack saturation in the sides of primary cracks was caused by the ECC fiber's hardening nature, which exhibits a strain-hardening response when the fiber is activated. Fig. 7b shows the fracturing contour for PVA-ECC fiber. Despite the higher strength and ductility of PVA-ECC compared to PP-FRC, the crack band of the PVA-ECC was narrower than that of the PP-FRC push-off specimen.

7. CONCLUSION

This paper has presented a numerical analysis of FRC that fails under combined shear and tensile loads. A custom stress-strain model for both fiber and plain concrete was proposed. The researchers employed an in-house 3D-NLFEA program to develop a multi-surface plasticity model to study the impact of the fiber's contribution on the deformation and shear strength of the simulated push-off specimen. It can be deduced from the numerical analysis that the specimen with 1.25 percent volumetric fiber content of PVA-ECC fiber exhibits the highest performance. PP fiber-containing specimens have significantly lower elastic moduli and exhibit substantial deformation even at elastic phases. The peak load-carrying capacity was nearly identical to that of the SFRC push-off specimen. Nevertheless, abrupt reductions in its capability to carry loads were detected once it had reached its maximum capacity.

The numerical simulation found that the push-off model made with steel-fiber reinforced concrete (SFRC) responds similarly to plain reinforced concrete (RC) but with a 72.48 % increase in load-carrying capacity. For the PVA-ECC FRC, the load-carrying capacity increased more than double (113.78 %) at a displacement of 5.20 mm. On the other hand, using PP-FRC can only slightly increase the load-carrying capacity (8.28 %). In addition, the PP-FRC has a much softer response during hardening due to lower elastic modulus than plain reinforced concrete push-off specimens.

It was discussed that the crack band for SFRC was more expansive than plain RC, indicating that the steel fiber resisted the crack growth. For PP-FRC, the fracturing contour was localized near the edge but did some propagation away from the crack localized area. Finally, the fracturing contour for PVA-ECC fiber showed a wider band of crack saturation and, therefore, can absorb higher inelastic energy.

8. ACKNOWLEDGMENTS

This research was funded by Badan Riset dan Inovasi Nasional (BRIN) and Lembaga Pengelola Dana Pendidikan (LPDP) under the scheme of Riset dan Inovasi untuk Indonesia Maju (RIIM) Batch 1 Year 2023. Research grant number: 22/IV/KS/06/2022 and 2127/PKS/ITS/2022. All authors of this manuscript are main contributors and have an equal primary role in conducting research.

9. REFERENCES

[1] Li V.C., Stang H., Elevating FRC material ductility to infrastructure durability. 6th RILEM Symposium on Fiber-Reinforced

Concretes (FRC) - BEFIB, Vol. 30, 2004, pp. 171–86 .

[2] Fischer G, Li V. C., Influence of matrix ductility on tension-stiffening behavior of steel reinforced engineered cementitious composites (ECC). Structural Journal, Vol. 99, Issue 1, 2002, pp. 104–111.

[3] Mohammed B. S., Khed V. C., Liew M. S., Optimization of hybrid fibres in engineered cementitious composites. Construction and Building Materials, Vol. 190, 2018, pp. 24–37.

[4] Fauzan, Yuliet R., Habibillah K., Agista G. A., Juliafad E., The effect of a combination of steel fiber waste tyre and crumb rubber on the mechanical properties of high-strength concrete. International Journal of GEOMATE, Vol. 25, Issue 111, 2023, pp. 238–45.

[5] Soehardjono A., Sabariman B., Wisnumurti, Wibowo A., Contribution of steel fibers on ductility of confined concrete columns. International Journal of GEOMATE, Vol. 23, Issue 97, 2022, pp. 188–195.

[6] Amalia, Setiawan Y., Tiyani L., Murdiyoto A., Effect of rice husk and steel fibers on self-compacting concrete properties. International Journal of GEOMATE, Vol. 25, Issue 108, 2023, pp.130–137.

[7] Banaay K. M. H., Cruz O. G. D., Muhi M. M., Engineered cementitious composites as a high-performance fiber reinforced material: a review. International Journal of GEOMATE, Vol. 24, Issue 106, 2023, pp. 101-110.

[8] Abbas S. A., Abdulridha A. A., Sabih S. M., Influence of polypropylene fiber on the bond strength between steel bar and concrete. International Journal of GEOMATE, Vol. 21, Issue 83, 2021, pp. 117-124.

[9] Gustavo J., Parra-Montesinos., High-Performance Fiber-Reinforced Cement Composites: An Alternative for Seismic Design of Structures. ACI Structural Journal. Vol. 102, Issue 5, 2005, pp. 668–675.

[10] Johal L. Shear transfer in reinforced concrete with moment or tension acting across the shear plane. PCI Journal, July-August, 1975, pp. 76-93.

[11] Yu K., Wang Y., Yu J., Xu S., A strain-hardening cementitious composites with the tensile capacity up to 8%. Construction and Building Materials, 2017, Vol. 137, pp. 410–419.

[12] Hamoodi A. Z., Zewair M. S., Ojaimi M. F., Shear Behavior of Fiber-Reinforced Concrete Beams: An Experimental Study. International Journal of GEOMATE, Vol. 21, Issue 86, 2021, pp. 167–179.

[13] Ahmed M. A., Chkheiwer A. H., Alhamaidah A., Structural torsional response behavior and prediction for steel fiber-recycled aggregate concrete beams. International Journal of GEOMATE, Vol. 21, Issue 87, 2021, pp. 1–10.

[14] Ranade R, Basaran C, Fakhri H., Ductile fiber-reinforced concrete for corrosion mitigation in reinforced concrete structures: experiments and theory, Newport News, VA: American Society of Naval Engineers, Mega Rust 2017, Naval Corrosion Conference, June, 2017, pp. 1–14.

[15] Foster R. M., Morley C. T., Lees J. M., Modified Push-Off Testing of an Inclined Shear Plane in Reinforced Concrete Strengthened with CFRP Fabric. Journal of Composites for Construction, Vol. 20, Issue 3, 2016, pp. 1–10.

[16] Li V. C., Mishra D. K., Naaman A. E., Wight J. K., LaFave J. M., Wu H-C., Inada Y., On the shear behavior of engineered cementitious composites. Advanced Cement Based Materials, Vol. 1, Issue 3, 1994, pp. 142–149.

[17] Piscesa B., Attard M. M., Samani A. K., 3D Finite element modeling of circular reinforced concrete columns confined with FRP using a plasticity-based formulation. Composite Structures, Vol. 194, 2018, pp. 478–493.

[18] Piscesa B., Attard M. M., Samani A. K., Three-dimensional Finite Element Analysis of Circular Reinforced Concrete Column Confined with FRP using Plasticity Model. Procedia Engineering, Vol. 171, 2017, pp. 847–856.

[19] Piscesa B., Attard M. M., Prasetya D., Samani A. K., Modeling cover spalling behavior in high strength reinforced concrete columns using a plasticity-fracture model. Engineering Structures, Vol. 196, 2019, p.109336.

[20] Menetrey P., Willam K. J., Triaxial failure criterion for concrete and its generalization. ACI Structural Journal, Vol. 92, Issue 3, 1995, p. 311–318.

[21] Chen W-F., Plasticity in reinforced concrete. J. Ross Publishing, 2007.

[22] Grassl P., Lundgren K., Gylltoft K., Concrete in compression: a plasticity theory with a novel hardening law. International Journal of Solids and Structures, Vol. 39, Issue 20, 2002, pp. 5205–5223.

[23] Grassl P, Jirásek M. Damage-plastic model for concrete failure. International Journal of Solids and Structures, Vol. 43, Issue 22, 2006, pp. 7166–7196.

[24] Papanikolaou V. K., Kappos A. J., Confinement-sensitive plasticity constitutive model for concrete in triaxial compression. International Journal of Solids and Structures, Vol. 44, Issue 21, 2007, pp. 7021–7048.

[25] Piscesa B., Attard M. M., Samani A. K., A lateral strain plasticity model for FRP confined

concrete. Composite Structures, Vol. 158, 2016, pp. 160–174.

[26] Piscesa B., Attard M. M., Samani A. K., Refined plasticity model for concrete stress-strain relationships part II: inclusion of size effect. 23rd Australasian Conference on The Mechanics of Structures and Materials (ACMSM23), Vol. 1, 2014, pp. 155–160.

[27] Piscesa B., Attard M. M., Samani A. K., Tangaramvong S., Plasticity Constitutive Model for Stress-Strain Relationship of Confined Concrete. ACI Structural Journal, Vol. 114, Issue 2, 2017, pp. 361–371.

[28] Hoover C. G., Bažant Z. P., Cohesive crack, size effect, crack band and work-of-fracture models compared to comprehensive concrete fracture tests. International Journal of Fracture, Vol. 187, Issue 1, 2014, pp. 133–143.

[29] Červenka J., Papanikolaou V. K., Three-dimensional combined fracture–plastic material model for concrete. International Journal of Plasticity, Vol. 24, Issue 12, 2008, pp. 2192–2220.

[30] Crisfield M. A., An arc ‐ length method including line searches and accelerations. International Journal of Numerical Methods Engineering, Vol. 19, Issue 9, 1983, pp. 1269–1289.

[31] CEA/DEN, EDF_R&D, OPEN_CASCADE. SALOME - The Open-Source Integration Platform for Numerical Simulation. http://www.salome-platform.org/ 2023.

[32] Hughes T. J. R., The finite element method: linear static and dynamic finite element analysis. Courier Corporation, 2012.

[33] Irawan C., Piscesa B., Tambusay A., Purnomo S., Santoso G., Suprobo P., Nonlinear finite element analysis of full-scale external post-tensioned concrete box girder at jacking and service. Proceedings of International Structural Engineering and Construction, ISEC Press, Vol. 10, 2023, pp. (STR-52)1–6.

[34] Ranjbaran A., Embedding of reinforcement in reinforced concrete elements implemented in DENA. Computer and Structures, Vol. 40, Issue 4, 1991, pp. 925–930.

[35] Ranjbaran A., Mathematical formulation of embedded reinforcements in 3D brick elements. Communications in Numerical Methods in Engineering, Vol. 12, Issue 12, 1996, pp. 897–903.

[36] Béton CE-I du, CEB-FIP model code 1990: Design code. Thomas Telford Publishing, 1993.

[37] Irmawan M, Piscesa B, Alrasyid H, Suprobo P. Numerical Modeling of Steel Fiber Reinforced Concrete Beam with Notched under Three-point Bending Test. Civil Engineering and Architecture, Vol. 10, Issue 7, 2022, pp. 3227–3242.

[38] Komara I, Suprobo P, Iranata D, Tambusay A, Sutrisno W. Experimental investigations on the durability performance of normal concrete and engineered cementitious composite. IOP Conference Series: Materials Science and Engineering, IOP Publishing, Vol. 930, Issue 012056, 2020, pp.1–11.